THE JOURNAL OF PHYSICAL CHEMISTRY Letters

Letter

Cite This: J. Phys. Chem. Lett. 2019, 10, 1471−1476

pubs.acs.org/JPCL

Decreasing Nanocrystal Structural Disorder by Ligand Exchange: An Experimental and Theoretical Analysis

Gabriel R. Schleder,*[,†,‡] Gustavo M. Azevedo,[¶,§] Içamira C. Nogueira,[∥] Querem H. F. Rebelo,[∥,⊥] Jefferson Bettini,[‡] Adalberto Fazzio,[‡,†] and Edson R. Leite*[,‡,#]

[†]Federal University of ABC (UFABC), Santo André, São Paulo 09210-580, Brazil

[‡]Brazilian Nanotechnology National Laboratory (LNNano)/CNPEM, Campinas, São Paulo 13083-970, Brazil

[¶]Brazilian Synchrotron Light Laboratory (LNLS)/CNPEM, Campinas, São Paulo 13083-970, Brazil

[§]Federal University of Rio Grande do Sul (UFRGS), Porto Alegre, Rio Grande do Sul 90040-060, Brazil

[∥]Federal University of Amazonas (UFAM), Manaus, Amazonas 69080-900, Brazil

[⊥]Federal University of Western Pará (UFOPA), Santarém, Pará 68035-110, Brazil

[#]Federal University of São Carlos (UFSCar), São Carlos, São Paulo 13565-905, Brazil

Supporting Information

ABSTRACT: Nanocrystals (NCs) present unique physicochemical properties arising from their size and the presence of ligands. Comprehending and controlling the ligand−crystal interactions as well as the ligand exchange process is one of the central themes in NC science nowadays. However, the relationship between NC structural disorder and the ligand exchange effect in the NC atomic structure is not yet sufficiently understood. Here we combine pair distribution function analysis from electron diffraction data, extended X-ray absorption fine structure, and high-resolution transmission electron microscopy as experimental techniques and first-principles density functional theory calculations to elucidate the ligand exchange effects in the ZrO_2 NC structure. We report a substantial decrease in the structural disorder for ZrO_2 NCs caused by strain rearrangements during the ligand exchange process. These results can have a direct impact on the development of functional nanomaterials, especially in properties controlled by structural disorder.

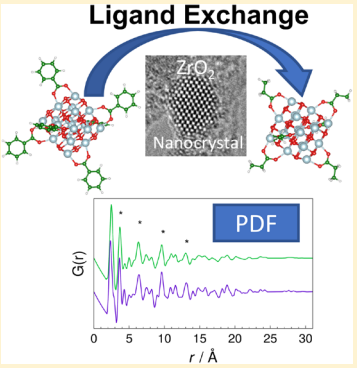

The size and presence of ligands in colloidal nanocrystals (NCs) are the main reasons why their physicochemical properties differ from the bulk crystal. The surface arising from the small size of the inorganic crystal is often capped by organic ligands, which determine the NCs' morphology and their colloidal stability.[1−4] Accordingly, the comprehension of and the control over the ligand-capped layer−inorganic crystal interaction have become central themes in the science of NCs. Recently, a significant advance has been achieved in understanding the chemical interactions between the ligand and the inorganic core, resulting in a covalent bond classification (CBC),[5−7] where the ligands are defined as L-, X-, or Z-type according to the number of electrons that the neutral ligand contributes to the inorganic core−ligand bond (2, 1, or 0, respectively). Also, recently, De Roo and coauthors[6,7] described a new class of NC−ligand system, named X_2. The CBC model allowed an advance in the surface ligand chemistry and opened a number of opportunities to design new reaction pathways for ligand exchange processes.

The ligands coordinate to surface atoms of the inorganic core, passivating the NC surfaces. During the ligand exchange process, atoms located at the surface will temporarily be less coordinated, resulting in increased electron sharing with the remaining bonds. Differently, when the new ligand binds to surface, a favorable coordination will be restored, creating the new passivated surface. During this process, reconstruction can take place, originating in a different structural disorder or defect density. The large proportion of surface atoms, as well as the presence of ligands, leads the NCs to show unusual forms of structural disorder. Gilbert et al.[8] quantitatively determined the structural disorder of ZnS nanoparticles, showing the existence of a heavily disordered surface region. On the contrary, Masadeh et al.[9] showed that the core structure of CdSe nanoparticles possesses a defined atomic arrangement without a significant disordered surface region, even for small particles of 2 nm. These findings highlight the complexity of the atomic arrangements in NCs.

Despite the progress achieved in the field of NC surface chemistry, the structural disorder of the inorganic core is still incompletely understood. Moreover, there is scarce information about the effect of the ligand exchange in this atomic structure. In this Letter, we address this issue, that is, how the ligand exchange modifies the structural disorder of the NCs. This characterization is highly relevant because passivation, as

Received: February 14, 2019
Accepted: March 14, 2019
Published: March 14, 2019

DOI: 10.1021/acs.jpclett.9b00439
J. Phys. Chem. Lett. 2019, 10, 1471−1476

well as the concentration and type of defects, may have a direct influence on the chemical, optical, and charge-transport behavior of the NC.

The determination of the atomic arrangements of nanomaterials is not a simple task, requiring the combination of several experimental characterization methods and theoretical calculations to support and achieve consistency in the structural analysis.[10,11] Here we combine pair distribution function (PDF), extended X-ray absorption fine structure (EXAFS), and high-resolution transmission electron microscopy (HRTEM) as experimental techniques and first-principles theoretical calculations based on density functional theory (DFT)[12] to elucidate the effect of the ligand exchange within ZrO_2 NCs and the consequent changes in the structural disorder.

The ZrO_2 NCs employed here were synthesized by a nonhydrolytic sol−gel-based process using the benzyl alcohol route. (For details, see the Supporting Information.)[13,14] This synthetic route leads to NCs where the core is formed by a tetragonal ZrO_2 phase with an organic ligand shell layer formed by RCCO− groups, where R is an aromatic ring.[15] For the ligand exchange process, the as-synthesized NCs were submitted to an extra solvothermal treatment, where the original ligand was replaced by an oleate ligand layer (oleic acid (OLA)).[16] After the exchange process, we obtained NCs with a ligand layer formed by R′CCO− groups, where R′ is now an unsaturated aliphatic chain. (For details regarding the ligand exchange procedure, see Figure S1.) Both ligands are X_2-type. The as-synthesized ZrO_2 NCs presented good dispersion in polar solvents such as ethanol. Contrarily, after ligand exchange, the ZrO_2 NCs showed a very high colloidal stability in nonpolar solvents, such as toluene and hexane.

HRTEM analysis of the ZrO_2 NCs before (named ZrNC−Benz) and after the ligand exchange process (ZrNC−OLA) shows the presence of individual NCs with no aggregates and the morphology of faceted and prolate particles (see Figure 1a,b). The detailed HRTEM image analysis (see inset in Figure 1a,b) revealed the formation of faceted ZrO_2 NCs with tetragonal symmetry, oriented along the ⟨010⟩ zone axis (see the fast Fourier transform analysis also in the inset of Figure 1a,b) for both nanoparticles. The statistical analysis of the particle size distribution from HRTEM images (Table 1) confirms the nonequiaxial morphology of the NCs. A mean larger diameter of 3.2 nm was measured for the ZrO_2 NCs both before and after the ligand exchange process. These results show that the ligand exchange process did not promote modification of the ZrO_2 NC size and shape as well of the crystalline phase.

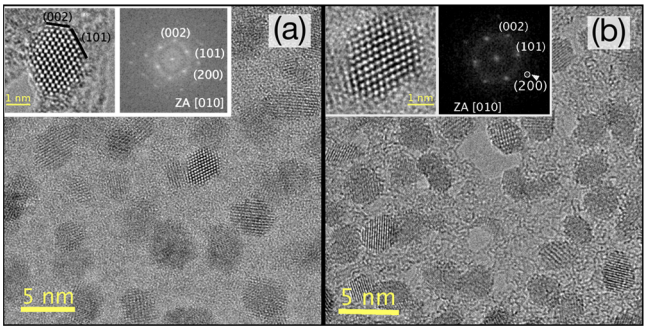

Figure 1. (a) HRTEM image of the ZrNC−Benz sample and (b) HRTEM image of the ZrNC−OLA sample. In both images, the insets shows an HRTEM image displaying the facets and the fast Fourier transform.

Table 1. Characteristic Sizes of the ZrO_2 NCs before and after the Ligand Exchange[a]

sample	mean larger dimension (nm)[b]	mean smaller dimension (nm)[b]	mean aspect ratio[b]
ZrNC−Benz	3.2	2.3	1.4
ZrNC−OLA	3.2	2.3	1.4

[a]Mean characteristic sizes were determined by measuring the size of at least 500 nanoparticles. [b]Because we are analyzing NCs with aspect ratio larger than 1 (with an approximate elliptical shape), we can define two characteristic dimensions, one along the axis with a large dimension (defined here as mean larger dimension) and another along the axis with smaller dimension (defined here as mean smaller dimension).

The ZrO_2 NC local structure was characterized by EXAFS measurements in the same samples analyzed by electron microscopy and PDF. EXAFS is an ideally suited technique for the analysis of the first nearest neighbors of a specific atomic species, given its chemical selectivity and short-range order sensitivity. EXAFS measurements were performed at the Zr K-edge at room temperature for the ZrO_2 NCs before and after the ligand exchange (see the experimental details and Figures S2 and S3), and the Fourier -transformed k^2-weighted spectra are shown in Figure 2. All spectra present the same spectral features and are consistent with the tetragonal ZrO_2 structure. The first peak centered around 1.5 Å (uncorrected for photoelectron phase shift) is composed of contributions from two Zr−O distances, which remain unmodified in the NCs as compared with the bulk standard. This reflects a fully coordinated first shell, composed of rigid Zr−O bonds, consistent with an oxygen-terminated nanoparticle surface, as proposed in Figure S7. On the contrary, the peak centered at 3.2 Å is dominated by two Zr−Zr distances and shows a significant reduction in the overall magnitude. The amplitude reduction relative to the bulk standard is due to the reduction average coordination number due to surface truncation. Considering the model presented in Figure S7, the average Zr−Zr coordination reduces from 12 in bulk to 9.2 in a 3.2 nm

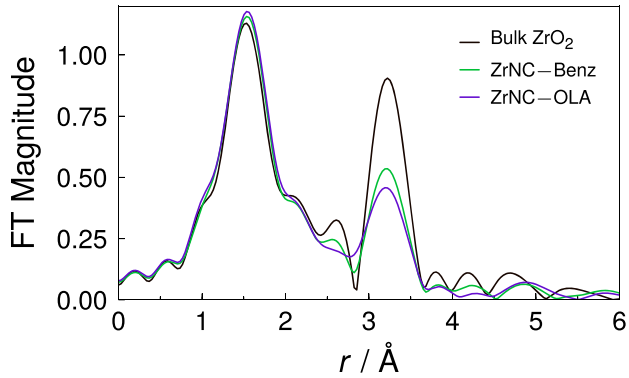

Figure 2. Non-phase-corrected magnitude of the Fourier transform of the k^2-weighted EXAFS signal obtained at the Zr K-edge for tetragonal bulk ZrO_2 and NCs samples (ZrNC−Benz and ZrNC−OLA). All spectra are consistent with the tetragonal structure of ZrO_2. The damping of the magnitude for the peaks centered around 3.2 Å can be ascribed to the shortening of Zr−Zr distances at the second coordination shell (see Table 2).

DOI: 10.1021/acs.jpclett.9b00439
J. Phys. Chem. Lett. 2019, 10, 1471−1476

nanoparticle. Differences between Benz- and OLA-capped nanoparticles can be ascribed to the shortening of one of the Zr−Zr distances at the second coordination shell, suggesting a degree of structural disorder in the NCs.

The structural parameters obtained in our fitting procedure are presented in Table 2 and can be summarized as follows.

Table 2. Structural Parameters Obtained from the Fitting Procedure, Considering a Tetragonal ZrO_2 Structure[17] [a,b]

EXAFS DATA − structural parameters (Zr K-edge)				
samples	Zr−O1 (Å)	$\sigma^2$1 (Å^2)	Zr−O2 (Å)	$\sigma^2$2 (Å^2)
bulk	2.078 (3)	0.0012 (4)	2.240 (4)	0.004 (1)
ZrNC−Benz	2.078 (4)	0.0015 (6)	2.229 (4)	0.004 (1)
ZrNC−OLA	2.075 (4)	0.0014 (7)	2.225 (5)	0.003 (1)
samples	Zr−Zr1 (Å)	$\sigma^2$1 (Å^2)	Zr−Zr2 (Å)	$\sigma^2$2 (Å^2)
bulk	3.59 (4)	0.009 (1)	3.63 (4)	0.009 (1)
ZrNC−Benz	3.51 (2)	0.008 (2)	3.63 (3)	0.008 (2)
ZrNC−OLA	3.47 (2)	0.008 (2)	3.62 (2)	0.008 (1)

[a]CIF File: 1526427 (Crystallography Open Database (COD), http://www.crystallography.net/). [b]Nearest neighborhood of Zr in the ZrO_2 tetragonal structure comprises two Zr−O and two Zr−Zr distances. In this Table, σ^2 stands for the Debye−Waller factor, and the number in parentheses is relative to the error of adjusted data. Coordination numbers for the Zr−Zr distances were fixed at 2.9 and 6.3.

The first coordination shell around Zr (Zr−O bonds) remains unchanged relative to the bulk standard, consistent with nanoparticles presenting oxygen-terminated surfaces. Static disorder, quantified by the Debye−Waller factors, is the same (within error bars) in nanoparticles and the bulk standard. The truncation of nanoparticle structure is manifested in the nearest Zr−Zr neighbors as a reduction in coordination numbers and contraction of distances. The latter result suggests that the nanoparticles are contracted along the *c* axis, consistent with trends indicated by our DFT calculations (see below).

We acquired electron diffraction (ED) patterns from the TEM experiments for ZrNC−Benz and ZrNC−OLA samples. From those patterns, we obtained the real-space interatomic distances correlation function, that is, the pair distribution functions (PDFs or $G(r)$). The ED patterns were used to generate the PDF because it requires a few micrograms of the sample and a short exposition time for data collection. (For more experimental details about the use of ED to generate PDF patterns, see the Supporting Information and Figures S4 and S5.)[18,19] The experimental PDF patterns of the ZrNC−Benz and ZrNC−OLA samples obtained from ED pattern are given in Figure 3a. Furthermore, a detailed analysis of the PDF patterns demands the comparison of the pattern obtained experimentally with a reference material. We used the following strategy to obtain the reference material: A DFT calculation[20−22] was performed to obtain the bulk ZrO_2 crystal with tetragonal symmetry (see the structure in Figure S6), and we truncated this crystal to generate an ideal NC (without relaxation accounting for nanoscale effects). We constructed the truncated NC following the same morphology (size and exposed facets) reported for the experimental ZrO_2 NCs observed in the HRTEM images (see Figure S7). On the basis of theoretical results (infinite crystal and truncated NC), we created the $G(r)$ pattern for the bulk ZrO_2 crystal and idealized ZrO_2 NC, which are displayed in Figure S8.

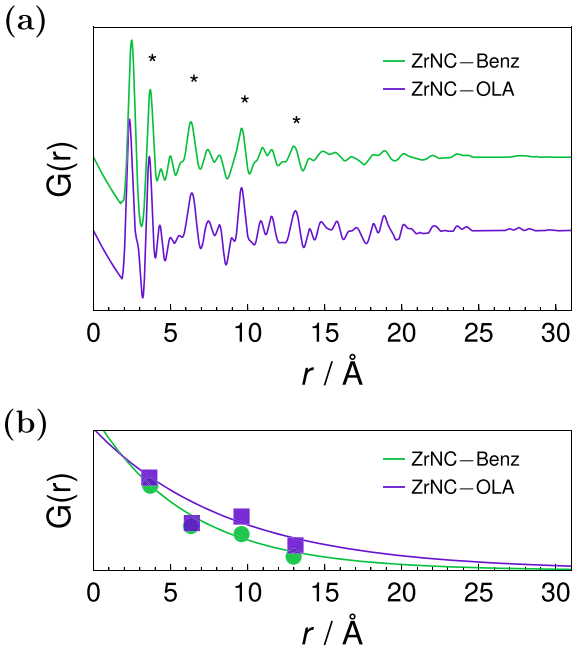

Figure 3. (a) Experimental $G(r)$ obtained from ED data for the ZrNC−Benz and ZrNC−OLA samples. The asterisks indicate the Zr−Zr peaks. (b) Fitting of the function $\exp(-\alpha r)$ to Zr−Zr peaks, used to perform a quantitative analysis of the LSC.

The $G(r)$ patterns for the bulk and idealized NC show a series of well-defined peaks, reflecting a specific atomic coordination sphere that is related to the tetragonal symmetry of the ZrO_2 crystals. The use of $G(r)$ patterns obtained from DFT calculations allowed peak indexing, according to the different pair correlated distances, such as Zr−O (distance between Zr and O atoms) and Zr−Zr (distance between Zr and Zr atoms). For instance, in Figure S8, we can see the total $G(r)$, as well as the Zr−Zr and Zr−O pairs, generated from the DFT calculations. Thus, for Figure 3a, we can attribute the first peak in the patterns, which is centered at ∼2.15 Å, as the first-neighbor Zr−O distance found in the tetragonal ZrO_2 crystal. We attribute the second peak around 3.5 Å to the Zr−Zr distance. These peak identifications agree with several published articles.[23−25] Because of the high symmetry of the tetragonal structure, we can easily identify the second-, third-, and fourth-neighbor Zr−Zr distances (see details in Figure 3a). We can also notice that the experimental PDF patterns present the features of the tetragonal symmetry.

From the PDF data, we can infer detailed structural information about the ZrO_2 NCs, as has been used for other nanomaterials.[26] In the idealized NC, the $G(r)$ peak intensity decays to zero at 3.2 nm, reflecting the finite length of structural coherence (LSC). Moreover, when we compare the patterns of the idealized NC with the ZrNC−Benz and ZrNC−OLA samples (Figure 3a), we note a smaller LSC for both ZrO_2 NCs, indicating the presence of structural disorder. This result agrees with the EXAFS analysis that showed the presence of this structural disorder in the Zr sublattice; that is, the structural disorder is associated with displacements in the Zr−Zr distances. We performed a quantitative analysis of the LSC for the ZrO_2 NCs following the approach developed by Ergun and Schehl[27] and the interpretation proposed by Petkov et al.;[28] that is, the LSC in the real NCs causes an exponential decay of the PDF peaks of the $\exp(-\alpha r)$ type, where *r* is the

DOI: 10.1021/acs.jpclett.9b00439
J. Phys. Chem. Lett. 2019, 10, 1471−1476

radial distance, so the average LSC = $2/\alpha$. The LSC has also been interpreted as the mean distance between defects.[27] We obtained the LSC by using the peaks assigned to the first-, second-, third-, and fourth-neighbor Zr−Zr distances of the $G(r)$ pattern. Figure 3b shows the plot of the Zr−Zr peak intensity as a function of r, where we can see a good agreement between the experimental data and the exponential decay function. From the fit, we obtained the LSC values of 1.1 and 1.7 nm for the ZrNC−Benz and ZrNC−OLA samples, respectively. Applying the same exponential decay model for the idealized NC, we found an LSC of 3.16 nm, showing the absence of structural disorder and confirming that the model used here describes well the LSC. (For details, see Figure S8c.) This is an interesting result. After the ligand exchange, the ZrO_2 NC shows a larger LSC; namely, we observe a decrease in the structural disorder. This large LSC region also has an impact on the PDF pattern. The PDF of the ZrNC−OLA showed more defined sharper peaks when compared with the ZrNC−Benz, indicating a better structuration of the NC and lower defect density after the ligand exchange process. Our PDF and EXAFS results clearly showed that there is a region in NCs with high crystallographic coherence, but this region is statistically small, showing that NCs have an extensive structural disorder mainly located on the NC surface. For instance, prior to the ligand exchange process, NCs had an equivalent coherent volume of only 8% (given by the LSC) relative to the NC total volume. After ligand exchange, we observed an increase of this volume to 28%. We consider that this static structural disorder is associated with lattice strain within NCs.[8,9,28] An extensive structural disorder has been reported in the literature for ZnS[8] and Fe_3O_4;[28] however, our results show that certain types of treatment can reduce the degree of disorder in the NCs, increasing the LSC.

Aiming to understand how the ligand exchange process modifies the degree of structural disorder of the ZrO_2 NCs, we performed DFT calculations of a tetragonal symmetry ZrO_2 cluster with size of ∼0.89 nm. In the ZrO_2 cluster, we bind the two different ligands (one where R is an aromatic ring and other where R′ is an unsaturated aliphatic chain). Figure 4a−c shows the models used. From the models after structural relaxation, we calculate the total and partial $G(r)$ curves (Zr−Zr and Zr−O pairs), and the resulting patterns are shown in Figure 4d. From the DFT calculations without and with different ligands (our model represents a nonstoichiometric cluster with oxygen deficiency on the surface), we obtained important information about the structure of this material. First, after relaxation, all clusters adopted a cubic symmetry and displayed a decrease in bond length, characteristic of nanoscale effects.[23,29] In the Supporting Information, including Figure S9, we present results concerning the effect of NC size on crystal symmetry, leading to a nonhomogeneous contraction. Second, the presence of the ligand decreases the chemical bond compressive strain, as we can observe in the $G(r)$ pattern pictured in Figure 4d. We can notice that the first peak relative to the Zr−O bond (at low r values) is insensitive to the ligand presence, whereas pairs at larger r values undergo a severe shift during the relaxation process. This shift is most evident for the Zr−Zr pairs. These data are strongly supported by the experimental EXAFS and PDF data reported here. These results indicate that the presence of the ligands releases the ZrO_2 lattice strain, which should then reduce the structural disorder. Finally, the ligand functional group type does not change the chemical bond length, as we see in Figure 4d. Still,

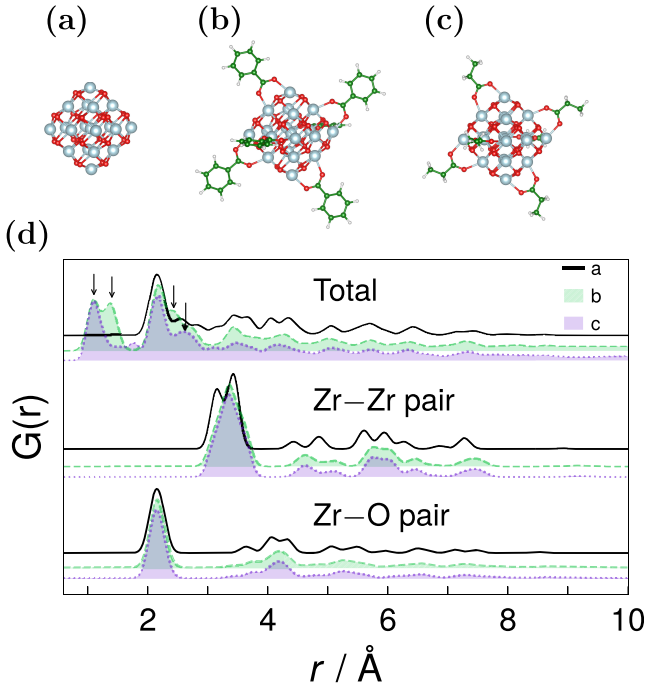

Figure 4. Structural models of (a) pristine ZrO_2 cluster, (b) ZrO_2 cluster with aromatic ligand, and (c) ZrO_2 cluster with aliphatic chain (C_2H_2−) ligand. Blue, red, green, and white represent Zr, O, C, and H atoms, respectively. (d) Total, Zr−Zr, and Zr−O $G(r)$ patterns of the clusters obtained from DFT calculations. The peaks indicated by arrows are assigned to the ligand atomic pairs.

when comparing the $G(r)$ curves for the two different ligands, differences in position or intensity of the peaks are not observed, showing that the type of organic radial group in the X_2 ligand does not interfere in the structure of the inorganic core. On the basis of this theoretical analysis, we can address some hypotheses to explain the structural disorder existence in the ZrO_2 NCs.

Following the theoretical analysis, we can reason that the structural disorder identified by EXAFS and PDFs is originated by the competition between the ZrO_2 NC bond length contraction tendency and the presence of ligands that decreases this strain of the chemical bonds. Regarding the restructuring effect for the ZrO_2 NCs promoted by the ligand exchange process, we notice that the X_2 ligand type has weak influence in the structural disorder decrease. The ZrO_2 NC structuring must be a consequence of the ligand's absence along with the high-temperature annealing process that occurs during the solvothermal treatment, which leads to reduced structural disorder, resulting in a larger LSC.

In conclusion, here we have demonstrated that the combination of advanced characterization techniques (EXAFS and PDF from ED) with theoretical DFT calculations is a powerful tool to reveal the nature of NC structures. We presented the unprecedented result that the ligand exchange process causes a decrease in the static structural disorder of the ZrO_2 NCs, mainly due to strain rearrangement caused by solvothermal treatment at elevated temperatures and not due to the type of functional organic group (R) present in the X_2-type ligand. These results have a direct impact on NCs manipulation processes involving ligands, properties associated with their structural disorder degree, and the development of functional nanomaterials, especially for functionalities where

DOI: 10.1021/acs.jpclett.9b00439
J. Phys. Chem. Lett. 2019, 10, 1471−1476

the structural disorder located on the surface plays an important role in the physicochemical properties, such as in mechanical, photoluminescence, electronic transport, and catalytic properties.

■ ASSOCIATED CONTENT

Supporting Information

The Supporting Information is available free of charge on the ACS Publications website at DOI: 10.1021/acs.jpclett.9b00439.

NC synthesis and ligand exchange details. EXAFS measurements and data analysis. HRTEM, ED, and PDF details. Electronic structure DFT calculations details (PDF)

■ AUTHOR INFORMATION

Corresponding Authors

*E.R.L.: E-mail: edson.leite@lnnano.cnpem.br.
*G.R.S.: E-mail: gabriel.schleder@ufabc.edu.br.

ORCID

Gabriel R. Schleder: 0000-0003-3129-8682

Notes

The authors declare no competing financial interest.

■ ACKNOWLEDGMENTS

We acknowledge financial support from the Fundação de Amparo à Pesquisa do Estado de São Paulo (FAPESP), project numbers 2017/18139-6, 17/02317-2, and CEPID 2013/07296-2. G.M.A. acknowledges financial support from the Conselho Nacional de Desenvolvimento Cientifico e Tecnológico (CNPq), project number 307806/2015-4.

■ REFERENCES

(1) Yin, Y.; Alivisatos, A. P. Colloidal nanocrystal synthesis and the organic−inorganic interface. *Nature* **2005**, *437*, 664−670.
(2) Park, J.; Joo, J.; Kwon, S. G.; Jang, Y.; Hyeon, T. Synthesis of Monodisperse Spherical Nanocrystals. *Angew. Chem., Int. Ed.* **2007**, *46*, 4630−4660.
(3) Boles, M. A.; Ling, D.; Hyeon, T.; Talapin, D. V. The surface science of nanocrystals. *Nat. Mater.* **2016**, *15*, 141−153.
(4) Pradhan, N.; Das Adhikari, S.; Nag, A.; Sarma, D. D. Luminescence, Plasmonic, and Magnetic Properties of Doped Semiconductor Nanocrystals. *Angew. Chem., Int. Ed.* **2017**, *56*, 7038−7054.
(5) Anderson, N. C.; Hendricks, M. P.; Choi, J. J.; Owen, J. S. Ligand Exchange and the Stoichiometry of Metal Chalcogenide Nanocrystals: Spectroscopic Observation of Facile Metal-Carboxylate Displacement and Binding. *J. Am. Chem. Soc.* **2013**, *135*, 18536−18548.
(6) De Roo, J.; Justo, Y.; De Keukeleere, K.; Van den Broeck, F.; Martins, J. C.; Van Driessche, I.; Hens, Z. Carboxylic-Acid-Passivated Metal Oxide Nanocrystals: Ligand Exchange Characteristics of a New Binding Motif. *Angew. Chem., Int. Ed.* **2015**, *54*, 6488−6491.
(7) De Roo, J.; Baquero, E. A.; Coppel, Y.; De Keukeleere, K.; Van Driessche, I.; Nayral, C.; Hens, Z.; Delpech, F. Insights into the Ligand Shell, Coordination Mode, and Reactivity of Carboxylic Acid Capped Metal Oxide Nanocrystals. *ChemPlusChem* **2016**, *81*, 1216−1223.
(8) Gilbert, B.; Huang, F.; Zhang, H.; Waychunas, G. A.; Banfield, J. F. Nanoparticles: Strained and Stiff. *Science* **2004**, *305*, 651−654.
(9) Masadeh, A. S.; Božin, E. S.; Farrow, C. L.; Paglia, G.; Juhas, P.; Billinge, S. J. L.; Karkamkar, A.; Kanatzidis, M. G. Quantitative size-dependent structure and strain determination of CdSe nanoparticles using atomic pair distribution function analysis. *Phys. Rev. B: Condens. Matter Mater. Phys.* **2007**, *76*, 115413.
(10) Billinge, S. J. L.; Levin, I. The Problem with Determining Atomic Structure at the Nanoscale. *Science* **2007**, *316*, 561−565.
(11) Petkov, V. Nanostructure by high-energy X-ray diffraction. *Mater. Today* **2008**, *11*, 28−38.
(12) Schleder, G. R.; Padilha, A. C. M.; Acosta, C. M.; Costa, M.; Fazzio, A. From DFT to Machine Learning: recent approaches to Materials Science − a review. *J. Phys. Mater.* **2019**, DOI: 10.1088/2515-7639/ab084b.
(13) Garnweitner, G.; Goldenberg, L. M.; Sakhno, O. V.; Antonietti, M.; Niederberger, M.; Stumpe, J. Large-Scale Synthesis of Organophilic Zirconia Nanoparticles and their Application in Organic−Inorganic Nanocomposites for Efficient Volume Holography. *Small* **2007**, *3*, 1626−1632.
(14) Deshmukh, R.; Niederberger, M. Mechanistic Aspects in the Formation, Growth and Surface Functionalization of Metal Oxide Nanoparticles in Organic Solvents. *Chem. - Eur. J.* **2017**, *23*, 8542−8570.
(15) Zhou, S.; Garnweitner, G.; Niederberger, M.; Antonietti, M. Dispersion Behavior of Zirconia Nanocrystals and Their Surface Functionalization with Vinyl Group-Containing Ligands. *Langmuir* **2007**, *23*, 9178−9187.
(16) Dalmaschio, C. J.; da Silveira Firmiano, E. G.; Pinheiro, A. N.; Sobrinho, D. G.; Farias de Moura, A.; Leite, E. R. Nanocrystals self-assembled in superlattices directed by the solvent−organic capping interaction. *Nanoscale* **2013**, *5*, 5602−5610.
(17) Igawa, N.; Ishii, Y. Crystal Structure of Metastable Tetragonal Zirconia up to 1473 K. *J. Am. Ceram. Soc.* **2001**, *84*, 1169−1171.
(18) Abeykoon, A. M. M.; Malliakas, C. D.; Juhás, P.; Bozin, E. S.; Kanatzidis, M. G.; Billinge, S. J. L. Quantitative nanostructure characterization using atomic pair distribution functions obtained from laboratory electron microscopes. *Zeitschrift für Krist.* **2012**, *227*, 248−256.
(19) Tran, D. T.; Svensson, G.; Tai, C.-W. SUePDF: a program to obtain quantitative pair distribution functions from electron diffraction data. *J. Appl. Crystallogr.* **2017**, *50*, 304−312.
(20) Hohenberg, P.; Kohn, W. Inhomogeneous Electron Gas. *Phys. Rev.* **1964**, *136*, B864−B871.
(21) Kohn, W.; Sham, L. J. Self-Consistent Equations Including Exchange and Correlation Effects. *Phys. Rev.* **1965**, *140*, A1133−A1138.
(22) Kresse, G.; Furthmüller, J. Efficient iterative schemes for ab initio total-energy calculations using a plane-wave basis set. *Phys. Rev. B: Condens. Matter Mater. Phys.* **1996**, *54*, 11169−11186.
(23) Gateshki, M.; Petkov, V.; Williams, G.; Pradhan, S. K.; Ren, Y. Atomic-scale structure of nanocrystalline ZrO2 prepared by high-energy ball milling. *Phys. Rev. B: Condens. Matter Mater. Phys.* **2005**, *71*, 224107.
(24) Gateshki, M.; Niederberger, M.; Deshpande, A. S.; Ren, Y.; Petkov, V. Atomic-scale structure of nanocrystalline CeO 2−ZrO 2 oxides by total x-ray diffraction and pair distribution function analysis. *J. Phys.: Condens. Matter* **2007**, *19*, 156205.
(25) Zhang, F.; Chupas, P. J.; Lui, S. L. A.; Hanson, J. C.; Caliebe, W. A.; Lee, P. L.; Chan, S.-W. In situ Study of the Crystallization from Amorphous to Cubic Zirconium Oxide: Rietveld and Reverse Monte Carlo Analyses. *Chem. Mater.* **2007**, *19*, 3118−3126.
(26) Schleder, G. R.; Fazzio, A.; Arantes, J. T. Oxidation of Ni_{13} Clusters. *Int. J. Quantum Chem.* **2018**, *119*, No. e25874.
(27) Ergun, S.; Schehl, R. R. Analysis of the structure of a glassy carbon using the fourier transform technique. *Carbon* **1973**, *11*, 127−138.
(28) Petkov, V.; Cozzoli, P. D.; Buonsanti, R.; Cingolani, R.; Ren, Y. Size, Shape, and Internal Atomic Ordering of Nanocrystals by Atomic Pair Distribution Functions: A Comparative Study of γ-Fe 2 O 3 Nanosized Spheres and Tetrapods. *J. Am. Chem. Soc.* **2009**, *131*, 14264−14266.

DOI: 10.1021/acs.jpclett.9b00439
J. Phys. Chem. Lett. 2019, 10, 1471−1476

(29) Puigdollers, A. R.; Illas, F.; Pacchioni, G. Structure and Properties of Zirconia Nanoparticles from Density Functional Theory Calculations. *J. Phys. Chem. C* **2016**, *120*, 4392−4402.

DOI: 10.1021/acs.jpclett.9b00439
J. Phys. Chem. Lett. 2019, 10, 1471−1476